ASPECTS REGARDING THE DEVELOPMENT OF AN ATMOSPHERIC IONIC PROPULSION PROTOTYPE USING ADDITIVE MANUFACTURING TECHNIQUES

Stefan Cristian CODREANU, Rares Alexandru SOCEA, George-Razvan BUICAN

"Transilvania" University of Brasov, Romania (stefan.codreanu@student.unitbv.ro)
rares.socea@student.unitbv.ro, buican.george@unitbv.ro)

DOI: 10.19062/2247-3173.2026.27.24

Abstract: *Ionic thrusters represent a category of engines that use electrical energy to generate thrust. Their operation is based on the Corona effect, an electrical phenomenon that occurs when an electrode carrying an electric current, at a sufficiently high voltage, generates an electric field strong enough to ionize the gas in the surrounding environment.*

This effect was discovered at the beginning of the twentieth century and was explained through the Drude–Lorentz theory, which states that metals are composed of multiple positively polarized nuclei among which valence electrons move. Thus, when a high-voltage electric current passes through an electrode, the gas molecules in the surrounding environment separate into positive ions and electrons, and their motion generates the ionic wind required to produce propulsive force.

Currently, ionic thrusters are used predominantly for equipping satellites, with the purpose of maneuvering them in the space environment. In this paper, we aim to physically develop such an ionic thruster, designed to operate in the atmospheric environment..

Keywords: *ionic thruster; atmospheric ionic propulsion; Corona effect; ionic wind; high-voltage electrode; gas ionization; additive manufacturing;*

1. INTRODUCTION

Electric propulsion, commonly referred to as ionic propulsion, is a method of accelerating a fluid by means of a high-voltage electric current, with the purpose of generating thrust through the achievement of high exhaust velocities. A significant consequence of this acceleration method is the substantial reduction in the quantity of propellant required during operation. As a result, the total weight of an aircraft or spacecraft is considerably reduced, which translates to lower operational costs over the vehicle's service life. [6]

The physical principle underlying electric propulsion is known as the Corona effect, a phenomenon that has been studied and developed by researchers since the 1920s. Its practical exploitation for space exploration began in the 1960s, and interest in this technology has grown consistently ever since. Electric propulsion, in its broadest definition, encompasses any propulsion system that employs electrical energy to accelerate the propellant. The key performance parameters of such systems are: thrust (measured in Newtons), specific impulse (Isp, measured in seconds), and overall thruster efficiency (η). [5]

The Corona effect is an electrical phenomenon that manifests around a high-voltage conductor through which a strong electric current passes.

The intense electric field generated around the conductor is sufficient to ionize the surrounding air. Once the critical discharge voltage is exceeded — approximately 19 kV in atmospheric air — air molecules are split into positive ions and free electrons. This mixture of ions and electrons is called plasma. Unlike a single continuous discharge such as lightning, the Corona effect produces a series of controlled micro-discharges whose characteristics depend on the geometry of the electrodes and the magnitude of the current passing through the conductor.

Optimizing the Corona effect requires both maximizing ionization efficiency and ensuring operator safety. This involves the correct selection of electrode geometry, operating voltage and current intensity, as well as maintaining the level of ozone generated below the permissible threshold. The present work aims to systematically investigate these parameters through an iterative experimental approach, coupling theoretical modelling with physical prototype development enabled by additive manufacturing.

2. SHORT HISTORY

The concept of ionic propulsion was first addressed in the early 20th century, starting with the development of the Drude-Lorentz theory of electron gases and the advancement of studies on the behaviour of electrically charged particles in electromagnetic fields. [1] The Drude-Lorentz theory, formulated in 1900, describes metals as composed of positively polarized ionic cores through which valence electrons move freely. This freedom of movement, made possible by electrostatic attraction forces between the positive cores and free electrons, implies that the ratio between electrical conductivity (σ) and thermal conductivity (κ) remains constant at a given temperature. [7]

$$\frac{\sigma}{k} = constant$$

The pioneer of electric propulsion is considered to be the Russian researcher Konstantin Tsiolkovsky, who, in the 1910s and 1920s, proposed using this type of propulsion for space missions. He worked alongside other prominent figures such as Hermann Oberth and Robert Goddard. [8] Goddard was the first to concretize electric propulsion theory and analyse its potential application in vacuum conditions, doing so as early as 1906. In 1926, Goddard achieved another landmark by launching the first liquid-propellant rocket to exceed the speed of sound. [2]

In 1924, Thomas Townsend Brown discovered the thrust force generated between two electrically charged objects, publishing his findings in an article titled 'How I Control Gravitation.' He described the creation of a 'Gravitator', an electric motor exploiting a phenomenon he termed 'electrogravitation,' comparing his device to a stack of high-voltage capacitors connected in series. One of Brown's conclusions involved an interaction between gravity and electromagnetism, a claim later disproved by subsequent experiments. These findings nonetheless contributed to the formulation of the Biefeld-Brown effect, which underpins modern electric propulsion: an asymmetric high-voltage capacitor produces a thrust directed toward the smaller electrode. [3]

In 1929, Hermann Oberth described a rocket propelled by accelerating electrically charged particles to high exhaust velocities using electric fields. He established the relationship between the required electrical power (P), the resulting thrust (T), and the exhaust velocity (vex) as: [2]

$$P = \frac{T * v_{ex}}{2}$$

This equation highlights the direct proportionality between required electrical power and thrust.

In 1948, British researchers Dr. L.R. Shepherd and A.V. Cleaver attempted to solve the onboard power generation problem — the same challenge faced by their predecessors — through the use of nuclear fission: a nuclear reactor would heat a fluid to high temperatures, which would then drive a turbine connected to an electrical generator. In 1954, Dr. Ernst Stühlinger proposed the development of a cesium-ion engine. [2]

By 1960, multiple government research programs had been established in both the United States (NASA) and the Soviet Union, aimed at developing electric propulsion for use in satellites and space stations. The first ionic thruster to be used in space was aboard the SERT-01 rocket, part of a joint US-USSR mission in 1964. Continued development led to the creation of Hall-effect thrusters, predominantly used by the Soviets during the Meteor communications satellite program. Japan introduced its first ionic thruster in 1995 aboard the ETS-VI communications satellite. [4]

The United States deployed its first ionic thruster in 1997 as part of the New Millennium program, aboard the Deep Space 1 spacecraft, which used photovoltaic energy generation. At the start of the 2000s, the Hughes/Boeing alliance launched the next generation of the XIPS (Hughes Xenon Ion Propulsion System) with a 25-centimeter diameter. In 2018, a joint ESA and JAXA mission to study Mercury's magnetic field and interior structure used electric propulsion aboard two satellites, marking one of the most complex electric propulsion missions to date. Most recently, in 2022, SpaceX utilized Hall-effect thrusters in its Starlink satellite launches. [5]

3. THE PURPOSE OF THE EXPERIMENT

The purpose of this experiment is to examine the Corona effect and to identify the critical parameters governing the performance of an ionic thruster. The research was motivated by the continued innovation in electric propulsion and the desire for a more thorough experimental examination of the Corona effect, drawing on the foundational work of pioneers such as Hermann Oberth, Thomas Brown, and Konstantin Tsiolkovsky, who identified electrical power input, specific impulse, exhaust velocity, and thrust as the essential performance metrics of ionic propulsion systems.

The specific parameters investigated in the course of this research are as follows:

- The voltage of the electric supply current (400 kV and 1000 kV transformer output levels).
- The distance between the emitter (anode) and the collector (cathode).
- The optimal emitter configuration in terms of number of ionization points.
- The influence of collector dimensions (cathode diameter: 15 mm, 22 mm, and 28 mm) on the resulting airflow exhaust velocity.

The experiment was designed to provide both a mathematical model of thruster behaviour and experimental validation through successive physical prototyping. The theoretical framework was complemented by mathematical modelling conducted using MATLAB R2025b, which was used to simulate the relationship between potentiometer position (i.e., supply voltage control) and the resulting thrust force for both transformer configurations.

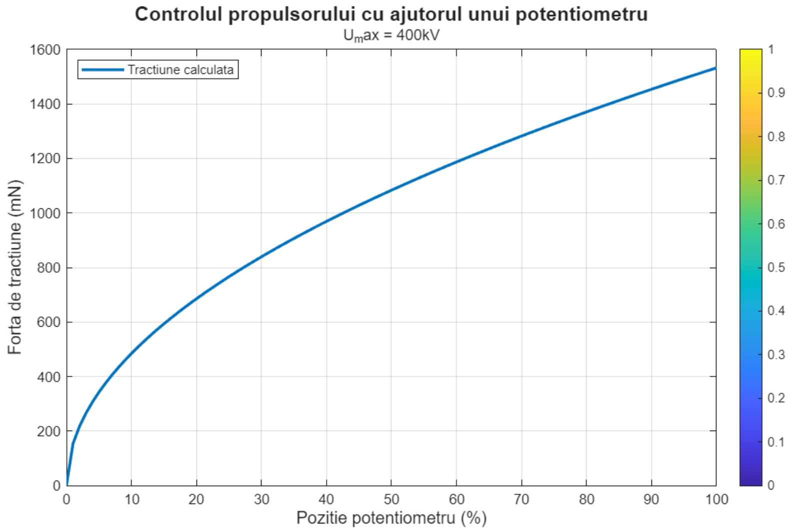

The variation of thrust, using the potentiometer, for the 400kV electrical current configurations

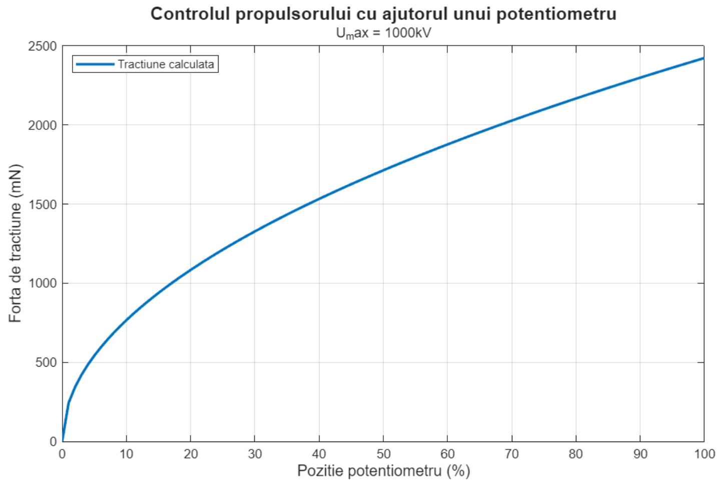

The variation of thrust, using the potentiometer, for the 1000kV electrical current configurations

4. THE EXPERIMENTAL HYPOTHESIS

Based on the observed development of electric propulsion systems and an analysis of their various operational configurations, three principal hypotheses were formulated prior to the execution of the experiments:

4.1 Hypothesis 1: Thrust is Proportional to Input Electrical Power

The generated thrust force is directly proportional to the input electrical power consumed by the device. Electrical power is expressed as $P = U * I$, where U is the supply voltage and I is the current intensity. For the Corona effect to occur, the supply voltage must exceed the critical discharge voltage in air: U ≥ Ucrt. The critical voltage is given by:

$$U_{crt} = m_0 * g_0 * \rho * r * \ln(\frac{d}{r})$$

where Ucrt is the critical Corona voltage, m_0 is the surface irregularity factor (equal to 1 for smooth, polished conductors), g_0 is the dielectric strength of air at standard pressure and temperature (~30 kV/cm), r is the conductor radius, d is the inter-electrode distance, and ρ is the air density factor depending on atmospheric pressure (p) and temperature (t): $\rho = 0.392 \times p / (273.15 + t)$. Assuming standard laboratory conditions (t = 20°C, p = 760 mmHg), for a conductor with a diameter of 1.5 mm and an inter-electrode distance of 10 mm, the critical voltage calculates to approximately 5.923 kV. The supply transformers used in this experiment (outputting 400 kV and 1000 kV) operate well above this threshold, ensuring reliable Corona discharge.

4.2 Hypothesis 2: Exhaust Velocity is Inversely Proportional to Inter-Electrode Distance

The exhaust velocity of the air current is inversely proportional to the distance between the emitter and the collector. During ionization, free electrons traveling from the anode to the cathode interact with air molecules, splitting them into positive ions and additional free electrons. Electromagnetic attraction and repulsion forces create a deceleration zone upstream of the cathode. The hypothesis states that a shorter inter-electrode distance results in weaker ion deceleration, due to the lower number of air molecules being ionized between the electrodes and, consequently, smaller attraction/repulsion forces within the plasma. This implies a higher net exhaust velocity for shorter electrode separations.

4.3 Hypothesis 3: Exhaust Air Velocity is Lower Than Plasma Velocity Between Electrodes

The exhaust velocity of the air downstream of the cathode is lower than the velocity of the plasma between the anode and the cathode. Near the cathode, the positive polarization of the electrode exerts a repulsive force on the approaching positive ions — stronger than the attractive force from free electrons being absorbed by the cathode. This creates a braking zone for positive ions just upstream of the cathode. While a portion of the ions overcome this zone due to inertia and are subsequently accelerated by electromagnetic repulsion after passing the cathode, the hypothesis holds that the net decelerating effect of the braking zone exceeds the accelerating effect of the repulsion force on the exhaust airstream. Consequently, the velocity of the ionic wind measured downstream is expected to be lower than the plasma velocity calculated between the electrodes.

5. MAIN COMPONENTS OF THE EXPERIMENTAL DEVICE

The experimental device developed in this research consists of three principal categories of components:

- The emitter (anode): the active component responsible for generating the ionic wind by creating and sustaining the Corona discharge. Various emitter configurations were tested, differing in the number and arrangement of ionization points (copper strands).
- The collector (cathode): the active component that intercepts the positive ions generated by the ionic wind. Three collector diameters were tested: 15 mm, 22 mm, and 28 mm. The collector features a planar interior surface facing the emitter to promote uniform ion collection.
- Support elements: structural components with low electrical conductivity, designed to hold the active components at defined relative positions. Initially fabricated from wood, these were subsequently replaced by components produced via additive manufacturing from PLA (Polylactic Acid).

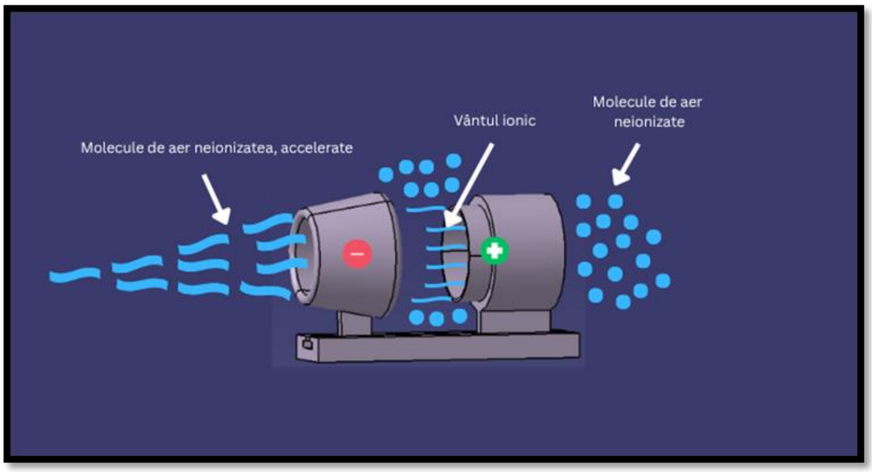

An example of an experimental device

The active components are manufactured from copper due to its excellent electrical conductivity. The emitter is constructed from copper pipe segments, with thin copper wires (strands) welded to the surface to create multiple ionization points. The collector is designed with a planar frontal surface to favour uniform ion collection.

The supply circuit consists of a type 18650 lithium-ion accumulator (3.7 V, 10 A, 3200 mAh, 47 g), a step-up voltage transformer (output: 400 kV or 800–1000 kV, supply: 3–6 V, weight: 53 g), an on/off switch, and — in later iterations — a linear potentiometer (10 kΩ, 3.3/5 VDC operating voltage, 90 × 20 mm) connected in series with the supply to allow fine-grained control of the output voltage and, consequently, of the thrust force.

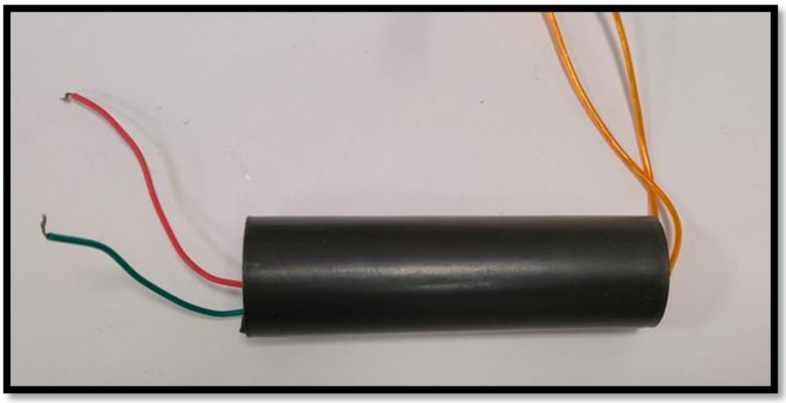

The 1000kV transformer used in the electrical circuit

6. THE MANUFACTURING OF THE DEVICE'S ACTIVE COMPONENTS

The development of the experimental device proceeded through six iterative design phases, each addressing the limitations of the previous configuration.

6.1 First Iteration

The initial concept adopted a circular cross-section for both the anode and cathode. Mathematical modelling of this first iteration drew on an analogy with a capacitor: the anode and cathode replaced the two armatures, and the surrounding air played the role of the dielectric.

The physical realization used copper cylindrical bushings as anode and cathode, with wooden support elements and alligator-clip connections to the supply circuit.

Upon testing, the exhaust velocity was found to be very low, observed using a smoke generator. Two probable causes were identified: the continuous (unpointed) inner surface of the anode, which lacked focused ionization points, and the alligator clips interfering with the generated airflow.

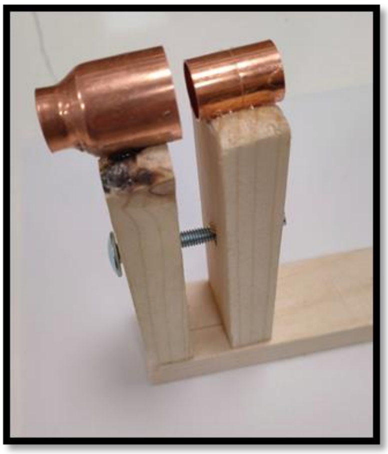

The first iteration of the experiment

6.2 Second Iteration

To address the deficiencies identified in the first iteration, the cylindrical copper bushing anode was replaced with a single insulated copper conductor whose end was stripped to expose 30 individual strands. By spreading the 30 strands apart, 30 discrete ionization points were created, with the expectation that these would generate more efficient ionization of the surrounding air than the continuous cylindrical surface. The same supply circuit components were retained. An exhaust velocity of 0.57 m/s was measured using a hot-wire anemometer probe. Residual sources of error included the non-uniform positioning of the anode (held by hand during the experiment) and variability in the probe position.

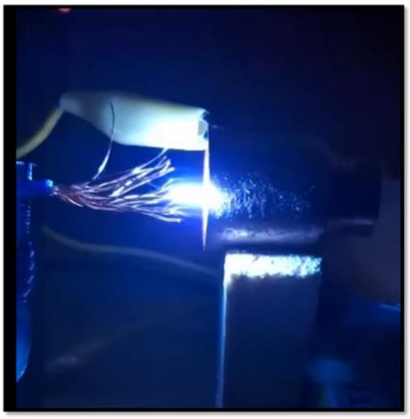

A sudden discharge during the experiment, using the second iteration

6.3 Third Iteration

The third iteration introduced a dedicated support structure for the anode and a fixed mounting for the measurement probe, eliminating the positional errors of the previous iteration.

The set of parameters to be systematically varied was formally established: inter-electrode distance, emitter geometry (number of ionization points: 4, 8, 16, 30, 60, and 90 strands), supply voltage (400 kV or 1000 kV), and cathode diameter (15 mm, 22 mm, and 28 mm).

A linear guide allowed the anode and cathode supports to be repositioned along the axial direction. The supply circuit was supplemented by two separate transformers. Measurement was performed using a KIMO AMI 300 hot-wire probe. Residual errors in this iteration included slight non-coaxiality between the anode and cathode due to lateral play between the supports and the guide, and vertical misalignment due to manufacturing tolerances in the bore holes. The experiment was also impeded by the rapid discharge of the 18650 accumulator, necessitating replacement approximately every 10 minutes.

6.4 Fourth Iteration — Introduction of Additive Manufacturing

The fourth iteration represented a major design overhaul, with all support components redesigned using CATIA V5 and manufactured via additive manufacturing (3D printing) to eliminate the dimensional inaccuracies of the hand-machined wooden supports. The material was changed from wood to PLA (Polylactic Acid).

The anode and cathode supports were redesigned as ring-with-leg elements, enabling secure fixture of the active components. These supports were inserted into intermediate support blocks featuring a central square-section bore, ensuring both coaxiality and parallelism of the electrode faces. The intermediate supports included a 6 mm lateral bore for fastening to the linear guide. The linear guide itself was redesigned as a plate incorporating a T-shaped channel that allowed the intermediate supports to be fixed at any position along the guide, with all other degrees of freedom constrained by the assembly geometry. The potentiometer was added to the supply circuit during this iteration to enable fine thrust control.

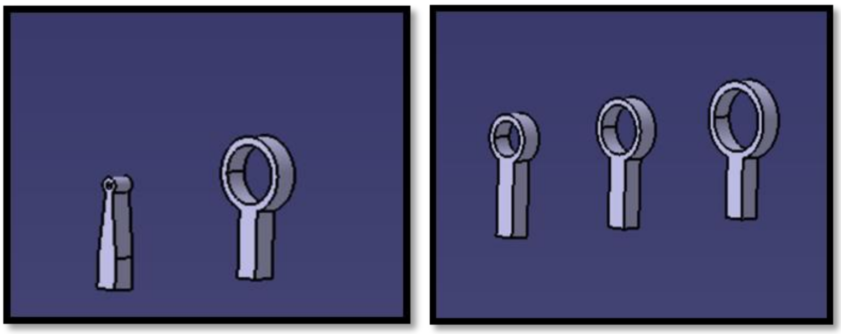

The supports of the active parts

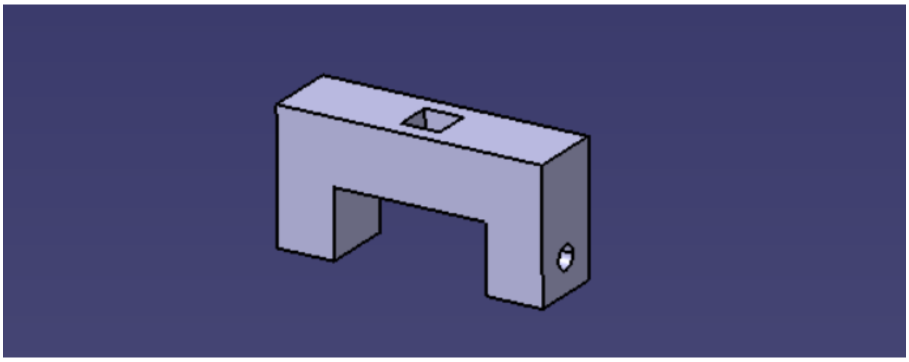

The intermediate support

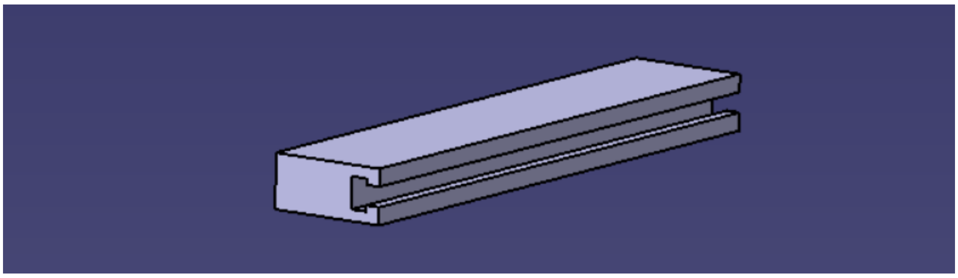

The linear guide, equipped with a T-channel

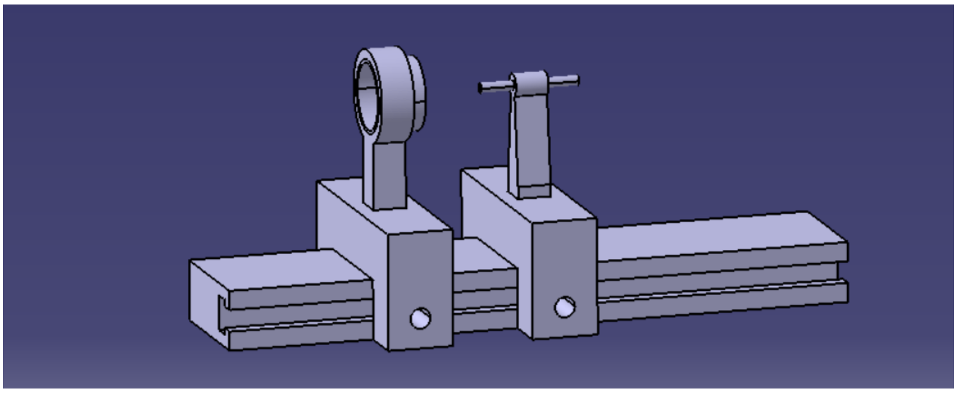

The final assembly of the experimental device

6.5 Fifth Iteration — Clustered Ionization Points

The fifth iteration explored an alternative arrangement of ionization points, concentrating them into clusters at diametrically opposite positions on the anode, rather than distributing them uniformly around the circumference. Anodes with 30, 60, and 90 ionization points arranged in bundles were fabricated and tested. The 30-strand anode from the fourth iteration was reused, while new anodes with 60 and 90 strands were manufactured. Due to their larger outer diameter, these anodes required new support elements with a clamping mechanism. The modular design of the intermediate supports and linear guide allowed their reuse without modification.

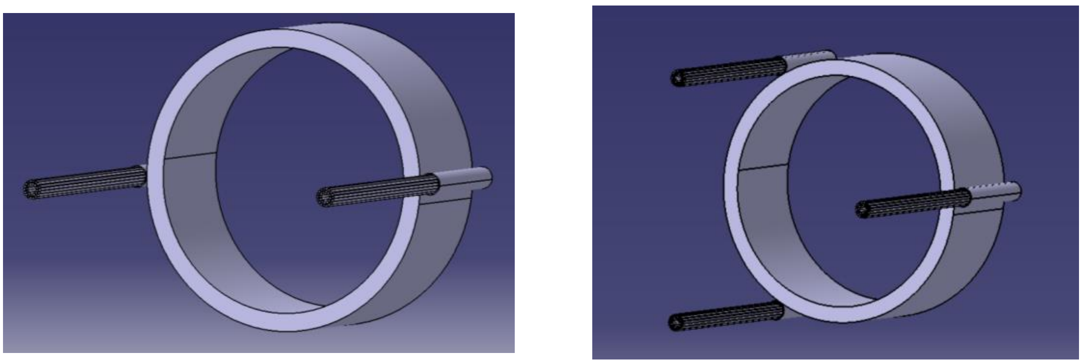

The 60 and 90-strand emitters

7. THE PRINTING PROCESS OF THE PASSIVE COMPONENTS

The additive manufacturing process used to produce the structural components of the experimental device was conducted in two distinct print runs, each using a different 3D printer configuration.

The first print run was performed using a Zortrax M200 Plus printer. The components were oriented horizontally on the print bed to reduce print time and improve dimensional accuracy. The total estimated print time for the first run was 20 hours and 37 minutes.

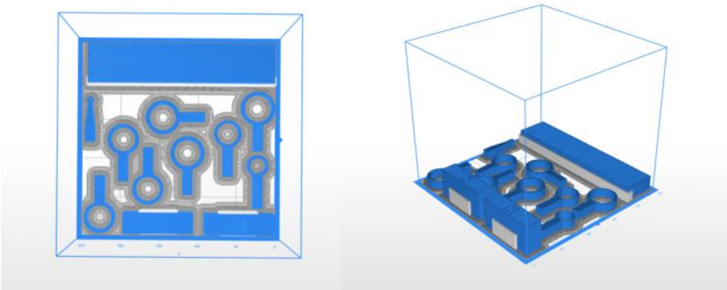

The placement of the passive components on the printer's table

After printing, material shrinkage of approximately 0.25 mm per side was observed in the bore diameters (designed at 6 mm, measured at 5.5–5.6 mm after printing), necessitating a post-print boring operation to restore the correct dimensions. Two main technological issues were identified after printing: the print support density was set too high, making removal extremely difficult — particularly inside the T-channel of the linear guide — and the blind square bores of the intermediate supports contracted by approximately 0.25 mm per side due to material shrinkage upon cooling, making the insertion of the active component supports impossible.

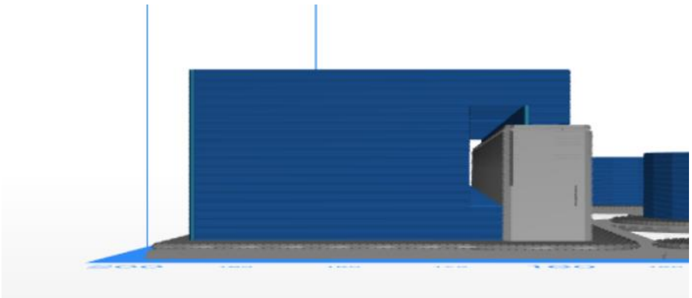

The first technological support of the T-channel

The second print run addressed both issues. The support block strategy was revised using 'Support Block' CAD elements in the printer's software to route the support structure away from the interior of the T-channel. The intermediate supports were also redesigned to account for the expected shrinkage. The second run was performed using a Tevo Tarantula printer. After the second print run, the components were assembled without the interference issues encountered previously. The complete experimental device, fully assembled, incorporated all redesigned 3D-printed elements alongside the active copper components.

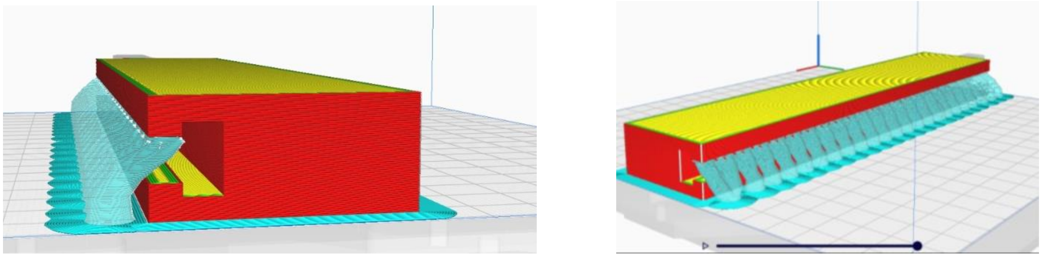

The second technological support of the T-channel

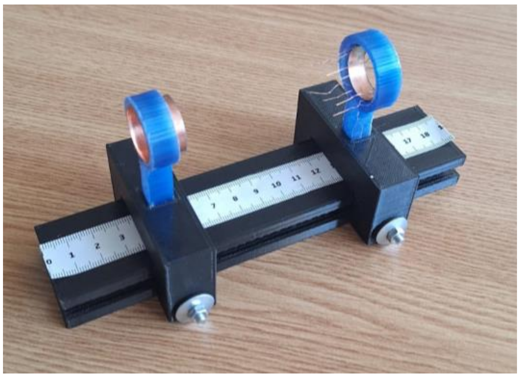

The final assembly of the experimental device

8. THE MEASURING OF THE EXPERIMENTAL DATA

Two primary parameters were tracked throughout the experimental campaign:

• The exhaust velocity of the air current generated by the ionic thruster.

• The ambient temperature during measurements, to account for any influence on the Corona effect and air density.

All measurements were performed using a KIMO AMI 300 hot-wire anemometer probe. The hot-wire probe operates by detecting the cooling effect of the airflow on a heated wire element, providing a direct measurement of flow velocity with high sensitivity at low velocities — particularly well-suited to the sub-meter-per-second velocities expected from the ionic thruster.

The experimental data were organized according to a Design of Experiments (DoE) Full-Factorial methodology. In a full-factorial design, all possible combinations of the selected factor levels are tested, ensuring that all main effects and interaction effects between variables can be identified and quantified. The independent variables (factors) were: supply voltage (2 levels: 400 kV, 1000 kV), inter-electrode distance (multiple levels), cathode diameter (3 levels: 15 mm, 22 mm, 28 mm), and number of ionization points on the anode (6 levels: 4, 8, 16, 30, 60, 90). The dependent variable (response) was the measured exhaust air velocity.

The hot-wire probe used in the measuring of the experimental data [9]

Factor	Levels	Level Values					
Ionization Points	6	4	8	16	30	60	90
Collector Diameter	3	15mm	22mm	28mm			
Emitter-Collector D	3	10mm	15mm	20mm			
Intake Voltage	2	400kV	1000kV				

The entry-data for the design of experiments phase [10]

9. THE RESULTS OF THE EXPERIMENT

The experimental results were compiled in a full-factorial data table and subsequently analysed through graphical representations designed to illustrate the dependence of exhaust velocity on each of the investigated parameters. The plots allowed the identification of optimal operating conditions and the verification of the pre-established hypotheses.

The relevant trends observed from the plots were as follows: increasing the supply voltage from 400 kV to 1000 kV consistently increased the measured exhaust velocity across all geometric configurations, broadly supporting Hypothesis 1. The effect of inter-electrode distance showed a general inverse trend with exhaust velocity, providing support for Hypothesis 2, though local variations were present due to the complex interaction between ion deceleration and plasma saturation effects. The relationship between the number of ionization points and exhaust velocity was non-monotonic: velocity initially increased as additional ionization points were added, but then decreased for very high ionization point counts (notably at 60 and 90 strands). This phenomenon was attributed to local air oversaturation between the electrodes — the excessive ionization depletes the available air molecules that can still be ionized, reducing the net thrust-generating plasma density.

10. THE CONCLUSIONS OF THE EXPERIMENT

The experimental campaign yielded the following principal findings:

•The maximum average exhaust air velocity was obtained for the following configuration: cathode diameter of 28 mm, inter-electrode distance of 15 mm, and supply voltage of 1000 kV.

•The exhaust air velocity decreases when the number of ionization points is increased beyond an optimal value, due to the oversaturation of the air between the electrodes. This finding is significant for the design of future prototypes, as it implies the existence of an optimal ionization density that maximizes thrust without causing self-limiting plasma depletion.

•The measured exhaust velocities confirmed the qualitative validity of all three hypotheses: thrust increases with input power, velocity decreases with increasing inter-electrode distance (at the tested range), and the downstream exhaust velocity is lower than the intra-electrode plasma velocity.

•The additive manufacturing approach proved highly effective for producing the structural components of the experimental device, enabling the tight tolerances required for electrode coaxiality, the complex geometry of the T-channel linear guide, and rapid iteration between design variants. Material shrinkage of PLA (~0.25 mm per side at 6 mm bore diameter) must be explicitly accounted for in the design phase.

•The modular design of the support structure (ring-with-leg active component supports, intermediate support blocks, and T-channel linear guide) allowed the rapid reconfiguration of the device between test configurations without requiring full disassembly, substantially accelerating the experimental campaign.

11. MAIN CONCLUSIONS

In the aerospace industry, additive manufacturing techniques represent one of the most significant technological innovations of the past decade. Their application in the context of ionic propulsion research demonstrated tangible advantages in terms of dimensional precision, design flexibility, speed of iteration, and cost of fabrication. The ability to produce geometrically complex structural components — such as the T-channel linear guide and the ring-with-leg electrode supports — from PLA with traditional subtractive manufacturing methods within the constraints of this research.

The advantages of additive manufacturing demonstrated in this work include: the ability to employ multiple materials (polymer, metal, and, in principle, ceramic), reduced manufacturing costs compared to conventional machining, and the production of high-precision components with complex internal geometries. PLA was found to be an appropriate structural material for the passive elements of the ionic thruster, combining adequate mechanical stiffness with excellent electrical insulation properties.

The ionic propulsion prototype developed in the course of this research successfully demonstrated the Corona effect as a viable atmospheric thrust-generation mechanism. Although the thrust magnitudes achieved at atmospheric pressure are modest compared to space-rated ionic thrusters operating in vacuum, the systematic experimental investigation of parameter interactions provides a valuable database for the design of next-generation prototypes and the development of more accurate analytical models.

From the broader perspective of electric propulsion research, this work confirms that the Corona effect's performance is highly sensitive to electrode geometry and electrical current. The identification of the air oversaturation phenomenon as a limiting factor for multi-point emitter configurations is a practically relevant result, suggesting that future emitter designs should optimize ionization point density rather than simply maximizing the number of points.

REFERENCES

[1] F. Alifano, M. Panelli și F. Battista, Preliminary Design Tool for Medium-Low-Power Gridded Ion Thrusters, 2023;

[2] “Propulsion for deep space”, June 1966;

[3] T.T. Brown, How I Control Gravitation, Science&Invention, August 1929;

[4] K. Holste, P. Dietz, S. Scharmann, K. Keil, *Ion thrusters for electric propulsion: Scientific Issues developing a niche technology into a gamer changer*, Rev. Sci. Instrum. 91, 061101, 2020;

[5] D. I. Boghiez, G. R. Buican, *Design and Experimental Evaluation of an Ion Engine Engine Prototype*, Review of the Air Force Academy, Vol. 23, No. 1, (51)/2025;

[6] G. R. Buican, R. C. Apreotesei, *Design and Experimental Evaluation of an Ion Wing Prototype*, AFASES 2025 Scientific Research and Education in the Air Force, Vol. 2025, 2025/5;

[7]https://asutoshcollege.in/new-web/Study_Material/Electric%20properties_Notes_6_23042020.pdf;

[8] https://en.wikipedia.org/wiki/Konstantin_Tsiolkovsky;

[9] https://www.nanasupplier.com/trirung-int/p-126729;

[10] https://numiqo.com/statistics-calculator/design-of-experiments/full-factorial-design-calculator.